Using Contours as Boundary Conditions for Elastic Registration during Minimally Invasive Hepatic Surgery

Nazim Haouchine, Frederick Roy, Lionel Untereiner, Stéphane Cotin

Using Contours as Boundary Conditions for Elastic Registration during Minimally Invasive Hepatic Surgery

Nazim Haouchine[1,2], Frederick Roy[1], Lionel Untereiner[1] and Stéphane Cotin[1,3]

***Abstract*— We address in this paper the ill-posed problem of initial alignment of pre-operative to intra-operative data for augmented reality during minimally invasive hepatic surgery. This problem consists of finding the rigid transformation that relates the scanning reference and the endoscopic camera pose, and the non-rigid transformation undergone by the liver w.r.t its scanned state. Most of the state-of-the-art methods assume a known initial registration. Here, we propose a method that permits to recover the deformation undergone by the liver while simultaneously finding the rotational and translational parts of the transformation. Our formulation considers the boundaries of the liver with its surrounding tissues as hard constraints directly encoded in an energy minimization process. We performed experiments on real *in-vivo* data of human hepatic surgery and synthetic data, and compared our method with related works.**

I. Introduction

Minimally invasive surgery techniques have been developed to positively impact the patients' post-operative and intra-operative outcomes. In this procedure, the surgery is performed using long instruments inserted through trocars located on the abdomen. The operating field is visualized through a laparoscopic camera inserted through the navel, allowing the surgeon to perform the operation by watching a monitor displaying the endoscopic images. With many benefits to the patients, such as reducing risks of hemoragging and bleeding as well as shortening time recovery, this surgical approach is now considered as a well-established procedure. However, since the manipulation of instruments is indirect and the visual feedback is limited, certain procedures remain quite challenging and require additional decision support such as surgery navigation. Naturally, the presence of a laparoscopic camera in the clinical routine has led the research community to investigate Augmented Reality (AR) techniques in order to align the preoperative models directly onto the surgeon's endoscopic view. During hepatic surgery, the objective is to facilitate the navigation by accurately locating tumors and vessels, to ensure hepatic function preservation.

Several approaches have been proposed to allow the use of AR during surgery. Most of the time they rely on a registration step that is often performed between a pre-operative model (usually a triangular 3D mesh) and points of interest (2D or 3D features) extracted from laparoscopic images [19], [23], [8], [24], [20]. However, although these methods have provided good results, the initial alignment is often done manually, thus restricting the practical uses of these methods in a surgical routine. Indeed, the initial alignment is a challenging problem for two main reasons: *(1)* only a partial view of the liver is visible on the endoscopic images and *(2)* the liver undergoes a large elastic deformation due to CO_2 insuflation (pneumoperitoneum [22]).

In this context, we propose a method that tackles the ill-posed problem of initial alignment by simultaneously estimating the rigid transformation of the endoscopic camera, and the elastic transformation of the liver.

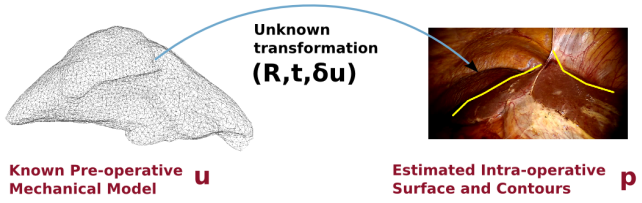

Fig. 1: Problem formulation: we aim at finding the transformation $\mathscr{T}$ corresponding to the rotation $\mathbf{R}$, the translation $\mathbf{t}$ and the deformation $\delta\mathbf{u}$, so that $\mathscr{T}(\mathbf{u}) = \mathbf{p}$. Our method is formulated as an energy minimization approach that minimizes the elastic energy between the pre-operative mechanical model and the intra-operative shape and boundaries.

II. Related Works

We can find in the literature several approaches that address the initial alignment issue. These approaches either try to enrich the intra-operative data by adding image constraints such as anatomical landmarks, additional imaging modality or position sensors, either try to estimate the organ deformation to obtain similar source and target mesh. Solving one of these two factors can reduce the problem to a 3D-3D registration for which a well-established method exists [14]. When dealing with the liver, estimating the deformation implies the simulation of the pneumoperitoneum that deforms the organs, and which is the source for the large misalignment between the preoperative data and intraoperative image. In [1] a simulation of the pneumoperitoneum is achieved using a biomechanical model in order to optimize the trocars placement on the skin. Pneumoperitoneum can also be modeled using mass-spring-damper models [15]. Gas insuflation is applied on the volume boundaries and the abdominal shapes are computed by solving the equations of motion. These methods provide accurate results for the whole abdominal system, with a high potential use for Augmented

[1]Inria, Mimesis project-team, Strasbourg, France
[2]nazim.haouchine@inria.fr
[3]stephane.cotin@inria.fr

Reality. However, it is more complicated to compute the correct shape of an organ on its own. Indeed, its boundaries, like attached ligaments, are not always known.

Recently, a database-based approach was proposed to simulate the liver deformation under pneumoperitoneum [10]. This database is built from intra-operative images and pre-operative segmentation, and is enriched with biomechanical boundary conditions.

Another way to solve the initialization problem is to rely on additional intra-operative data. In [5], the authors use an intra-operative ultrasound probe to register the vessel tree on a three dimensional liver model. The registration of the vessels drives the deformation of the whole organ and thus approximates the pneumoperitoneum. Oktay *et al.* [16] suggested to exploit intra-operative CT-scans after insufflation as an additional constraint to drive the simulation. Recently [2], a method proposed to scan the tip of the endoscopic camera to find its rigid pose w.r.t the intra-operative scanned organs. The superimposition of the 3D model with the images was tested clinically on porcine liver showing accurate results. These methods provide accurate registration but rely on intra-operative scans which are not available in actual clinical routines.

In order to counteract the practical limitations of additional intra-operative imaging, some methods choose to only rely on laparoscopic images acquired from the camera. Clements *et al.* [3] introduced a registration approach that uses salient anatomical features, identifiable in both the pre-operative images and intra-operative liver surface data. This method is able to reach a reasonable solution, but is limited to rigid transformations. In a similar context, Plantefeve *et al.* [18] proposed a non-rigid solution based on anatomical atlases to gather information about feature positions. These methods are based on manual estimation of anatomical structure positions which are cumbersome to be done in a clinical context [19]. Beside anatomical landmarks, organ silhouette was recently considered [4], [21]. The organ silhouette can indeed bring powerful information and better constrain the registration process.

We choose in this study to rely only on laparoscopic images acquired from the camera towards the intra-operative side, and on an elastic biomechanical model built from pre-operative data. The contributions of the paper are threefold. First we present an automatic approach for extracting liver contours using a structural point cloud clustering. We then extrapolate the acquired data in order to model the pneumoperitoneum, that will be considered as boundary conditions. We finally propose an energy minimization solution that simultaneously finds the rigid and non-rigid transformations in a single expression.

III. Problem formulation

Let us denote $\mathbf{u} = \{u_i \in \mathbb{R}^3\}, i \in \{1 \dots n\}$ the positions (volume's degrees-of-freedom) of the biomechanical model at rest configuration in the pre-operative stage and $\mathbf{p} = \{p_i \in \mathbb{R}^3\}, i \in \{1 \dots m\}$ the positions of the intra-operative image-points of the liver after pneumoperitoneum deformation.

We seek to find the transformation $\mathscr{T}$ that gives:

$$\mathscr{T}^{\mathbf{R},\mathbf{t},\delta\mathbf{u}}(\mathbf{u}) = \mathbf{p} \tag{1}$$

where $\mathbf{R}$ and $\mathbf{t}$ are respectively the 3×3 rotation matrix and 3×1 translation vector that represent the rigid transformation, and $\delta\mathbf{u}$ is a $3n$ vector of nodal displacements which encodes the elastic deformations of the intra-operative biomechanical model $\mathbf{p}$.

IV. Contour detection and 3D shape estimation

A. 3D shape estimation from stereoscopy

Exploiting laparoscopic images to extract useful information represents a critical step in our method. Indeed, performing a coherent registration highly depends on the quality of the target segmentation. In our case, this target represents the 3D shape of the liver and has to be recovered from 2D laparoscopic images. In order to estimate this shape, that we denote $\mathbf{s} = \{s_i \in \mathbb{R}^3\}$, we rely on well-established stereoscopy techniques [9], where a pair of images is provided using pre-calibrated stereo-endoscopes. Without loss of generality, we use a sparse matching algorithm that permits to find correspondences between image pairs. After filtering out mismatched points using epipolar constraints and unicity criterion, these correspondences are triangulated to finally generate the 3D point cloud $\mathbf{s}$.

This 3D point cloud is scattered, noisy and contains outliers due to the hidden parts between detected coutours. We thus need to build a 3D surface, denoted $\mathbf{s}^*$, which does not contain outliers and fits $\mathbf{s}$. Indeed, the surface must reflect the complex geometry of the scene. For this purpose, we use instead a Cocone surface reconstruction algorithm [6] that, in contrast to widely used smoothing algorithms [11], preserves the initial geometry, especially curvature and normals.

B. Contour detection using structures from point cloud

The surface $\mathbf{s}^*$ gives a 3D representation of the whole intra-operative scene. In order to separate the different components of the scene, we propose a classification method based on the surface curvature. Knowing the bending characteristic of the intra-operative scene, the idea is to find strong bending discontinuities that represent the frontiers between anatomical regions using a region growing scheme.

(a) (b) (c)

Fig. 2: Detection of the liver upper and lower boundaries using structures from point cloud: from the intra-operative view (a) we reconstruct a 3D map using stereoscopy (b) and based on bending curvatures we extract the contour of the liver. These contours are used as hard constraints in the problem formulated in Eq. 1

Let us denote $\mathbf{v} = \{v_i \in \mathbb{R}^3\}$ the set of vertices of the surface $\mathbf{s}^*$ and c_{v_i} the mean curvature of v_i. Using a region growing method, we classify the set of vertices $\mathbf{v}$, starting from a set of seed points $\mathbf{d} = \{d_i \in \mathbb{R}^3\}$ and growing through neighbors based on curvature criterion. The seed points are first selected to be the points with the lowest curvatures c_{min}, representing the flat regions. From the seed point, the set of neighbours $\mathbf{v}^* = \{v_i^* \in \mathbb{R}^3\}$ are examined so that the angle between the seed point d_i and its neighbor v_j^* is below a certain threshold ϑ_{th} following $cos^{-1}(|(c_{d_i}, c_{v_j^*})|) < \vartheta_{th}$. In this case, the neighbor v_j^* is added to the current region. Once it is tested for all the neighbors, if the curvature of a neighbor is smaller than a curvature threshold c_{th}, this neighbor is added to the set of seed points $\mathbf{d}$ while the seed point d_i is removed.

C. Abdominal modelling

This step reconstructs the neighborhood of the liver in order to define the surrounding tissues as boundary conditions. It requires therefore to model the anatomical parts that the endoscopic camera cannot capture. More precisely, the surface $\mathbf{s}^*$ is composed of different not connected components, labelled according to the tissue they belong to. To reconstruct the tissue boundaries located behind the liver, we extrapolate the surface visible in the camera view.

Let us first explain our method on a two-dimensional example (figure 3). Using a region growing method, we are able to determine the points that lie on the frontier with the liver (figure 3.b). Then, we compute the tangent line of these boundary points (see figure 3.c), and finally, this tangent line is used to compute a line that follows the direction given by the tangent (see figure 3.d).

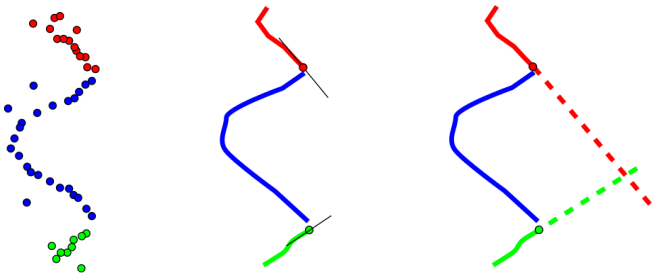

(a) (b) (c)

Fig. 3: Abdominal geometrical modelling (in 2D representation) with, (a) the detected and labelled contours in the endoscopic image, (b) the surface reconstruction using Cocone with the tangent line of frontier points and (c) the final boundaries with extrapolated hidden parts.

This method extends naturally to the third dimension by replacing the line reconstruction by a plane reconstruction. Thus, a tangent plane is computed for each point on the border of the meshes surrounding the liver. Knowing the equation of the planes one can compute a surface mesh. Using the diaphragm, the stomach, and liver partial surfaces, our algorithm defines three surface boundaries representing a closed volume $\mathbf{p}$.

V. Energy minimization

Let us return to the estimation of the transformation $\mathscr{T}$ corresponding to the rotation $\mathbf{R}$, the translation $\mathbf{t}$ and the deformation $\delta\mathbf{u}$. It can be expressed as an energy minimization problem where the solution is the equilibrium between the internal forces of the biomechanical model $\mathbf{u}$ and the external forces that emanate from the intra-operative image-based mesh $\mathbf{p}$.

A. Elastic model

Preliminary studies often considered the liver as an elastic body governed by Newton's second law $\mathbf{M\ddot{u}} = \mathbf{f}(\mathbf{u})$, where $\mathbf{M}$ is the mass and $\mathbf{f}$ is a non-linear function of the position $\mathbf{u}$ that represents the sum of internal and external forces and $\ddot{\mathbf{u}}$ is the acceleration. Solving this partial differential equation of motion is done through numerical methods using the Finite Element Method (FEM). In the FEM framework, the liver is represented as a volumetric mesh consisting of 3D polyhedra called elements. We choose here to use therahedral elements with linear shape functions. Since we do not focus on the transient part of the deformation but rather the static equilibrium under some specific loading, we consider a quasi-static integration scheme canceling the dynamic effects, which lead to the system $\mathbf{f}(\mathbf{u}) = 0$, that can be solved through a time-step linearization of the form:

$$\mathbf{f}(\mathbf{u} + \delta\mathbf{u}) = \mathbf{f}(\mathbf{u}) + \mathbf{K}(\mathbf{u})\delta\mathbf{u} \tag{2}$$

where $\mathbf{K}(\mathbf{u})$ is a Jacobian matrix called the stiffness matrix that represents the internal forces of the liver. Following the work of [17], we use the co-rotational formulation introduced by Felippa in [7] which allows large displacements while relying on a linear expression of the stress-strain relationship. The co-rotational approach is based on the decomposition of the actual element configuration into rotational and deformational components, both being quantified w.r.t. the initial position. With this approach, the force acting on the element e is defined as $\mathbf{f}_e = \mathbf{R}_e^\top \mathbf{K}_e(\mathbf{R}_e\delta\mathbf{u})$, where $\mathbf{R}_e$ is the rotation matrix of the element e and $\mathbf{K}_e$ is the element's stiffness matrix. Finally, the global matrix $\mathbf{K}$ is formed by assembling the element's stiffness matrices $\mathbf{K} = \sum_e \mathbf{K}_e$. The equation of a deformation of the liver will therefore take the general form:

$$\mathbf{K}\delta\mathbf{u} = \mathbf{f} \tag{3}$$

Here $\mathbf{K}$ is a matrix of size $3n \times 3n$ built depending on the elastic properties of the liver, the Young's modulus and the Poisson's ratio, while $\mathbf{f}$ is a vector of size $3n$ corresponding to the external forces.

B. Boundary conditions

We propose to consider the extended contours s as boundary conditions of the mechanical system. These contours are

expressed as stiff forces acting on the physical volume to enforce the elastic registration, following

$$\sum_{i}^{m} \frac{1}{2} k \|p_i - \mathbf{R}u_i - \mathbf{t}\|^2 \tag{4}$$

where k is the stiffness coefficient of the liver shape, the diaphragm and the bottom structures. The value of k is empirically chosen to be the same orders of magnitude as the Young's Modulus.

C. Volume conservation constraint

We add to the system a volume conservation constraint, so that the liver deformation remains realistic. Assuming V_i is the initial volume computed from the pre-operative stage and V_d the volume of the model during the deformation, this constraint is simply written as:

$$\|V_d - V_i\|^2 \leq \varepsilon \tag{5}$$

Note that this constraint does not influence the mechanical behaviour of the model and is considered as a stop criteria rather than a hard constraint.

D. Global minimization

Finally, the cost function is written so that, *1)* it satisfies the boundary constraints, where the projection of the mesh on the images should result in a minimal distance error, *2)* it ensures the conservation of the volume and *3)* it reaches equilibrium between the internal and external forces of the mechanical model. This leads to the following minimization

$$\min_{\mathbf{R},\mathbf{t},\delta\mathbf{u}} \left(\frac{1}{2} \|\delta\mathbf{u}^\top \mathbf{K} \delta\mathbf{u}\| + \sum_{i \in m} \frac{1}{2} k_i \|p_i - \mathbf{R}u_i - \mathbf{t}\|^2 \right) \tag{6}$$

This minimization can be efficiently solved using an iterative conjugate gradient solver.

E. System Initialization

The convergence of the system is sensitive to the initial values of $\mathbf{R}$ and $\mathbf{t}$. In order to find a rough estimation of these initial values, that we denote $\mathbf{R}_0$ and $\mathbf{t}_0$, we propose to use a heuristic based on the surgical approach. Indeed, one can notice a repeated pattern in the surgical view where the camera is inserted through the navel heading the lungs and both left and right lobes are observed. Using this pattern, detecting the separation of the left and right lobes on the laparoscopic images can easily be done with the help of an operator and on pre-operative data using atlases transfer. This anatomical landmark permits to obtain a rough estimation of the translation where the camera position and orientation can bring an additional cue to constrain the rotation. Moreover, assuming a subset of l points extracted from $\mathbf{p}$ and $\mathbf{u}$ corresponding to the anatomical landmark denoted p_i^* and u_i^* respectively. Finding $\mathbf{R}_0$ and $\mathbf{t}_0$ amounts at minimizing the quantity

$$\min_{\mathbf{R}_0,\mathbf{t}_0} \sum_{i \in l} \left[\|p_i^* - \mathbf{R}_0 u_i^* - \mathbf{t}_0\|_F^2 + \cos^{-1}(c_{cam}, c_{u_i^*}) \right] \tag{7}$$

where c_{cam} is the normal vector corresponding to the camera position and $c_{u_i^*}$ is the normal vector of the anatomical landmark.

VI. Results

We present in this section the results obtained using our method on synthetic and *in-vivo* surgical data. We compare our image-based elastic registration **IDBC** with the following methods: the well-known coherent point drift **CPD**, a probabilistic approach for non-rigid registration of noisy, partial and deformed point clouds and an anatomical-landmark-based approach **AL** for non-rigid liver registration.

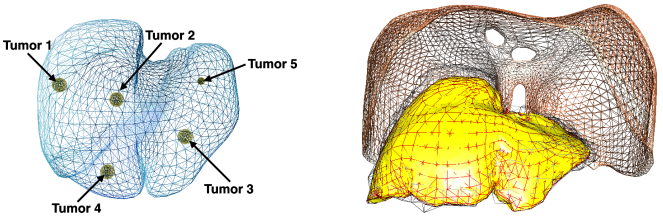

(a) (b)

Fig. 4: Dataset of the synthetic data experiments: (a) the locations of the tumors in the rest configuration of the liver (b) result of the registration.

A. Synthetic data

We evaluated our method, by measuring the registration error on inner structures such as tumors. Using the framework SOFA [1] we simulated the diaphragm and the liver under pneumoperitoneum, illustrated in figure 4. We considered 5 tumors at different locations (near the surface and in-depth). From the simulated data we extracted the shape of the liver where we added a Gaussian noise with standard deviation of 10 mm and a 5 % clustering decimation. We calculated the error as the Euclidean distance between the simulated tumors and the measured ones using our method.

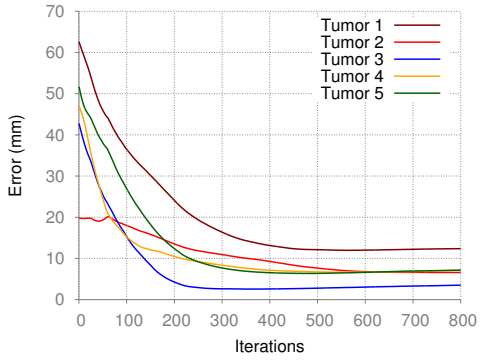

Fig. 5: Registration error for synthetic data experiments.

The results reported in Fig. 5 show the registration error for each tumor. Depending on the location of the tumors, we measured a distance error ranging from 4 to 12 mm. Note

[1] http://www.sofa-framework.org

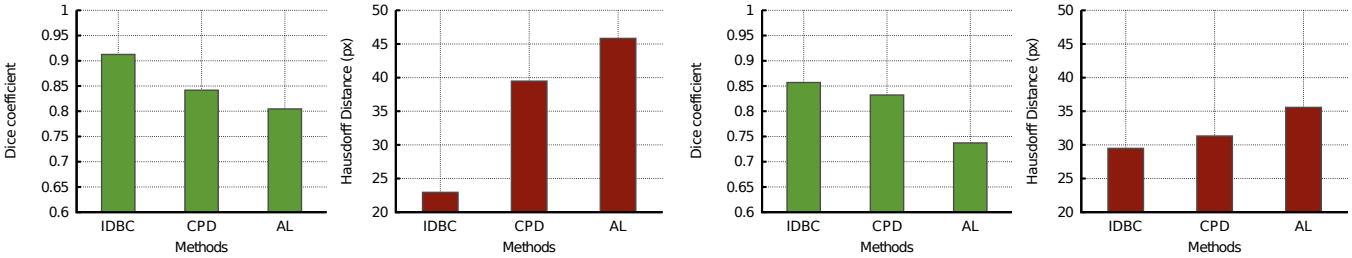

(a) View 1: Dice coefficient (b) View 1: Hausdorff distance (c) View 2: Dice coefficient (d) View 2: Hausdorff distance

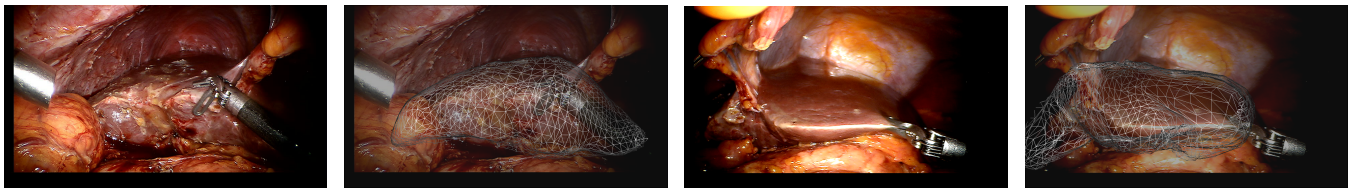

(e) **Input** (f) **IDBC (ours)** (g) **Input** (h) **IDBC (ours)**

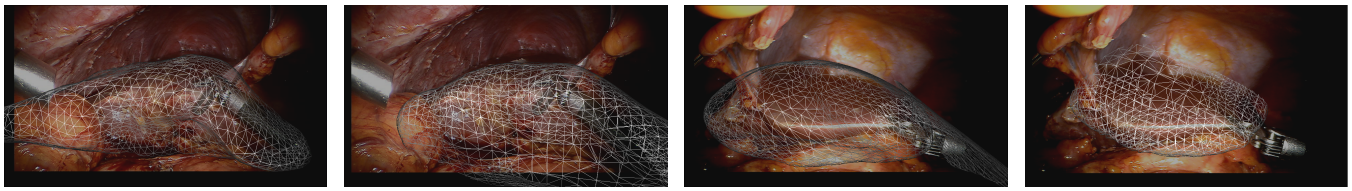

(i) **CPD** (j) **AL** (k) **CPD** (l) **AL**

Fig. 6: Experiments conducted *in-vivo* on human liver data with view 1 and view 2 using the methods **IDBC (ours)**, **CPD** and **AL**. Figures (a) and (c) show the Dice coefficient where (b) and (d) show the Hausdorff distance. Figures (e) and (g) show the input images. Figures (f), (h), (i), (j), (k) and (l) show the superimposition results.

that these results are obtained after the computation of $\mathbf{R}_0$ and $\mathbf{t}_0$.

B. Surgical Data

Obtaining a ground truth that describes human liver under pneumoperitoneum during minimially invasive surgery involves performing an intra-operative CT scan, which is actually not possible for ethical and practical reasons. To counteract this limitation we propose to compute the Dice similarity measure and the Hausdorff distance between the silhouette of the registered mesh and the manually segmented liver contour.

We used elastic parameters according to [17], [8]. The Young's modulus of parenchyma $E = 27$ KPa and Poisson's ratio $\mu = 0.45$. The model was composed of 3391 linear P1 tetrahedral elements. The simulation was running stably at a refresh rate of 25 FPS. Endoscopic images of size 960×540 px were acquired from a Da Vinci robot endoscopic camera (Intuitive Surgical), at a framerate of 29.97 fps. We used the SIFT [12] algorithm for feature extraction and matching of the stereoscopic image pair.

The results reported in figure 6 show that **IDBC** gives the highest similarity score and lowest distance error using the Hausdorff measure w.r.t to **CPD** and **AL**.

a) View 1: In this view, only the right lobe is visible in the intra-operative image along with the diaphragm, the falciform ligament and surgical instruments. A Dice similarity of 0.91 and an Haussdorf distance of 22.95 px for **IDBC**. The coherent point drift and the anatomical landmark method give a lower Dice coefficient, 0.84 and 0.80, and a higher Hausdorff distance, 39.47 px and 45.82 px for **CPD** and **AL** respectively.

b) View 2: This view represents the left lobe surrounded by ligament tissue and bottom fat. We report a Dice similarity of 0.85 and an Haussdorf distance of 29.48 px are measured for **IDBC**. The **CPD** and **AL** methods give relatively close results with a Dice similarity of 0.83 and 0.73, and a Hausdorff distance of 31.31 px and 35.57 px respectively.

C. Computational Time

Computation time is considered as one of the most critical aspects of computer-aided surgery. In our case, a high computation rate is needed to allow real-time augmentation of pre-operative data where several surgical events may occur and thus intra-operative updates are necessary.

	Computational time (seconds)		
Methods	**IDBC (ours)**	**CPD**	**AL**
View 1	9.8	44.8	260.6
View 2	76	191.8	553.4

TABLE I: Comparison of the computational time for each of the above-mentioned methods.

To demonstrate the ability of our method to provide an accurate registration while being computationally cheap, we measured the computation time reported in table I. The results show that in addition to have the lower computation time w.r.t to **CPD** and **AL**, **IDBC** can reach convergence relativity fast and can encounter the surgical routines requirements. Besides, our results were obtained with an Intel i7 3.5Ghz processor. Therefore, even faster results can be expected with higher configurations.

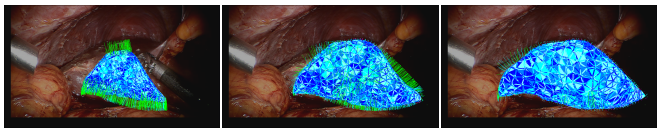

t = 0 s **t = 5 s** **t = 10 s**

Fig. 7: Selected frames of our method performed on an *in-vivo* human liver: we can notice the progressive registration between the FEM pre-operative model, in blue, and the intra-operative contours of the liver. The green lines represent the distance to the contours.

VII. Conclusion

We addressed in this paper the ill-posed problem of initial registration of pre-operative to intra-operative data for augmented reality during minimally invasive hepatic surgery. We proposed a method capable of simultaneously finding the rigid transformation of the endoscopic camera pose, and the elastic transformation arising from the pneumoperitoneum. Our method involves the automatic detection of liver boundaries through the segmentation of intra-operative 3D point cloud. From these boundaries a series of surface patches are generated using mesh processing techniques to model the pneumoperitoneum. These surface patches are used as boundary conditions for a biomechanical liver model. Promising results, i.e. lower errors compared to related works, were obtained through *in-vivo* experiments on a human liver. In addition, fast computation is achieved, making our approach compatible with surgical practice. More validation is obviously required though it is worth mentioning that validation implying actual organs are seldom reported in previous works. The integration of a complete biomechanical model as presented in [8] is planned in our future works. A sensitivity study on material parameters will be conducted, where recent studies [13] suggest that patient-specific properties are not necessary. Improving the estimation of the diaphragm surface and hidden parts will also be addressed.

References

[1] J. Bano, A. Hostettler, S. A. Nicolau, S. Cotin, C. Doignon, H. S. Wu, M. H. Huang, L. Soler, and J. Marescaux. Simulation of pneumoperitoneum for laparoscopic surgery planning. In *Proceedings of the 15th MICCAI: Part I*, pages 91–98, 2012.

[2] S. Bernhardt, S. A. Nicolau, V. Agnus, L. Soler, C. Doignon, and J. Marescaux. Automatic detection of endoscope in intraoperative ct image: Application to ar guidance in laparoscopic surgery. In *Biomedical Imaging (ISBI), 2014 IEEE 11th International Symposium on*, pages 563–567, April 2014.

[3] L. W. Clements, W. C. Chapman, B. M. Dawant, R. L. Galloway, and M. I. Miga. Robust surface registration using salient anatomical features for image-guided liver surgery: Algorithm and validation. *Medical Physics*, 35(6):2528–2540, 2008.

[4] T. Collins, D. Pizarro, A. Bartoli, M. Canis, and N. Bourdel. Computer-assisted laparoscopic myomectomy by augmenting the uterus with pre-operative mri data. In *Mixed and Augmented Reality (ISMAR), 2014 IEEE International Symposium on*, pages 243–248, Sept 2014.

[5] B. Dagon, C. Baur, and V. Bettschart. A framework for intraoperative update of 3d deformable models in liver surgery. In *IEEE EMBS*, pages 3235–3238. IEEE, 2008.

[6] T. K. Dey and J. Giesen. Discrete and computational geometry: The goodman-pollack festschrift. chapter Detecting Undersampling in Surface Reconstruction, pages 329–345. Springer Berlin Heidelberg, 2003.

[7] C. A. Felippa. A study of optimal membrane triangles with drilling freedoms. *CMAME*, 192(16-18):2125–2168, 2003.

[8] N. Haouchine, J. Dequidt, I. Peterlik, E. Kerrien, M.-O. Berger, and S. Cotin. Image-guided simulation of heterogeneous tissue deformation for augmented reality during hepatic surgery. In *ISMAR 2013*, pages 199–208, 2013.

[9] R. I. Hartley and A. Zisserman. *Multiple View Geometry in Computer Vision*. Cambridge University Press, ISBN: 0521540518, second edition, 2004.

[10] S. F. Johnsen et al. Database-based estimation of liver deformation under pneumoperitoneum for surgical image-guidance and simulation. In *Medical Image Computing and Computer-Assisted Intervention - MICCAI 2015*, pages 450–458, 2015.

[11] D. Levin. The approximation power of moving least-squares. *Math. Comput.*, 67(224):1517–1531, Oct. 1998.

[12] D. G. Lowe. Distinctive image features from scale-invariant keypoints. *Int. J. Comput. Vision*, 60(2):91–110, Nov. 2004.

[13] K. Miller and J. Lu. On the prospect of patient-specific biomechanics without patient-specific properties of tissues. *Journal of the Mechanical Behavior of Biomedical Materials*, 27:154 – 166, 2013.

[14] A. Myronenko and X. Song. Point set registration: Coherent point drift. *IEEE Trans. Pattern Anal. Mach. Intell.*, 32(12):2262–2275, Dec. 2010.

[15] Y. Nimura et al. Pneumoperitoneum simulation based on mass-spring-damper models for laparoscopic surgical planning. *Journal of Medical Imaging*, 2(4):044004, 2015.

[16] O. Oktay et al. Biomechanically driven registration of pre- to intra-operative 3d images for laparoscopic surgery. In *Proceedings of the 16th MICCAI: Part II*, pages 1–9, 2013.

[17] I. Peterlik, C. Duriez, and S. Cotin. Modeling and real-time simulation of a vascularized liver tissue. In *Proceedings of the 15th MICCAI*, pages 50–57, 2012.

[18] R. Plantefeve, N. Haouchine, J.-P. Radoux, and S. Cotin. Automatic alignment of pre and intraoperative data using anatomical landmarks for augmented laparoscopic liver surgery. In *International Symposium on Biomedical Simulation*, volume 8789 of *LNCS*, pages 58–66, 2014.

[19] R. Plantefève, I. Peterlik, N. Haouchine, and S. Cotin. Patient-specific biomechanical modeling for guidance during minimally-invasive hepatic surgery. *Annals of Biomedical Engineering*, 44(1):139–153, 2016.

[20] D. C. Rucker, Y. Wu, L. W. Clements, J. E. Ondrake, T. S. Pheiffer, A. L. Simpson, W. R. Jarnagin, and M. I. Miga. A mechanics-based nonrigid registration method for liver surgery using sparse intraoperative data. *IEEE Transactions on Medical Imaging*, 33(1):147–158, Jan 2014.

[21] A. Saito, M. Nakao, Y. Uranishi, and T. Matsuda. [poster] deformation estimation of elastic bodies using multiple silhouette images for endoscopic image augmentation. In *Proceedings of the 2015 IEEE International Symposium on Mixed and Augmented Reality*, ISMAR '15, pages 170–171, 2015.

[22] F. M. Sánchez-Margallo, J. L. Moyano-Cuevas, R. Latorre, J. Maestre, L. Correa, J. B. Pagador, L. F. Sánchez-Peralta, J. A. Sánchez-Margallo, and J. Usón-Gargallo. Anatomical changes due to pneumoperitoneum analyzed by mri: an experimental study in pigs. *Surgical and Radiologic Anatomy*, 33(5):389–396, 2011.

[23] D. Santos et al. Pose-independent surface matching for intra-operative soft-tissue marker-less registration. *Medical image analysis*, 18(7):1101–1114, 2014.

[24] S. Suwelack et al. Physics-based shape matching for intraoperative image guidance. *Medical physics*, 41(11):111901, 2014.